Advances in Aircraft and Spacecraft Science, *Vol. 7, No. 6 (2020) 553-570*
DOI: https://doi.org/10.12989/aas.2020.7.6.553

Modeling and coupling characteristics for an airframe-propulsion-integrated hypersonic vehicle

Chengkun Lv[1], Juntao Chang*[1], Yilei Dong[1], Jicheng Ma[1] and Cheng Xu[2]

[1]Harbin Institute of Technology, 150001 Heilongjiang, People's Republic of China
[2]Science and Technology on Complex System Control and Intelligent Agent Cooperation Laboratory, 100074 Beijing, People's Republic of China

(Received February 6, 2020, Revised August 20, 2020, Accepted August 23, 2020)

Abstract. To address the problems caused by the strong coupling of an airbreathing hypersonic vehicle's airframe and propulsion to the integrated control system design, an integrated airframe-propulsion model is established, and the coupling characteristics between the aircraft and engine are analyzed. First, the airframe-propulsion integration model is established based on the typical nonlinear longitudinal dynamical model of an air-breathing hypersonic vehicle and the one-dimensional dual-mode scramjet model. Thrust, moment, angle of attack, altitude, and velocity are used as transfer variables between the aircraft model and the engine model. The one-dimensional scramjet model can accurately reflect the working state of the engine and provide data to support the coupling analysis. Second, owing to the static instability of the aircraft model, the linear quadratic regulator (LQR) controller of the aircraft is designed to ensure attitude stability and height tracking. Finally, the coupling relationship between the aircraft and the engine is revealed through simulation examples. The interaction between vehicle attitude and engine working condition is analyzed, and the influence of vehicle attitude on engine safety is considered. When the engine is in a critical working state, the attitude change of the aircraft will not affect the engine safety without considering coupling, whereas when coupling is considered, the attitude change of the aircraft may cause the engine unstart, which demonstrates the significance of considering coupling characteristics.

Keywords: airframe-propulsion integration model; linear quadratic regulator; airframe-propulsion coupling characteristics; interaction between vehicle attitude and engine working condition

1. Introduction

Airbreathing hypersonic vehicles have become one of the important development directions in the field of aerospace technology (Burcham *et al.* 1998, Smith *et al.* 1990). An airbreathing hypersonic vehicle typically has a tightly integrated airframe and propulsion system. In order to deal with the strong coupling characteristics of the airbreathing hypersonic vehicle, it is essential to carry out an integrated design. This is the premise and foundation upon which to establish a model that reflects the performance and safety characteristics of the engine (Andrew *et al.* 2006, Yao *et al*. 2010).

At present, there are two typical integration models in the published literature. The first model was established by Chavez and Schmidt (1994) from the Aerospace Research Center of the

*Corresponding author, Ph.D., E-mail: changjuntao@hit.edu.cn

http://www.techno-press.org/?journal=aas&subpage=7 ISSN: 2287-528X (Print), 2287-5271 (Online)

University of Arizona. The second model was established by Bolender and Doman (2005). The latter model is more accurate and complex than the former. These two models conceptually embody the strong coupling nature of the airbreathing hypersonic vehicle, but the engine models are all zero-dimensional. A zero-dimensional model is also called a lumped parameter method. It assumes that the parameters are homogenized throughout the engine. Zero-dimensional models are widely used to analyze the overall performance of engines (Mitani *et al.* 1997, Roux and Tiruveedula 2016). However, a scramjet has extremely strongly distributed parameter characteristics over the whole flow field. A zero-dimensional model does not represent the complicated working mechanism of a scramjet, and thus it cannot obtain the accurate working conditions of the engine and accurately analyze the coupling characteristics between the aircraft and the engine. If the control system uses a zero-dimensional model, it may obtain unreliable information, which would render the control system unable to complete the control task (McClinton 2006, Hank *et al*. 2007).

A dual-mode one-dimensional model of a scramjet engine for control and real-time simulation was established by Ma (2019). Unlike the zero-dimensional model used by previous researchers, the one-dimensional model can reflect the physical processes inside the engine and the distributed parameter characteristics in the engine flow field (Cui 2014, Lee 2015), and can obtain the real engine performance parameters and safety margin, which can be used to accurately analyze the coupling characteristics between the aircraft and the engine. It can also be used for control system design (Parker *et al*. 2007, Bharani *et al*. 2010). Based on the one-dimensional model, the integrated modeling and coupling characteristics are analyzed in this study. Many control methods have been used to control hypersonic vehicles (Zuppardi 2015, Liu and Hua 2015, Xu 2015, Shen *et al.* 2018, Wang *et al.* 2019, Zhou *et al* 2019), LQR control was used in this study. LQR theory is an early and mature state space design method in modern control theory, which is easy to form the closed-loop optimal control by state linear feedback. Groves *et al*. (2005) discussed two linear quadratic optimal control methods, setpoint tracking control and regulator control, for the air-breathing hypersonic vehicle. Considering the saturation characteristic of the control input, the anti-windup control for statically unstable system was proposed by LQR method (Groves *et al.* 2006). Huo *et al.* (2006) described an adaptive linear quadratic (ALQ) altitude and velocity tracking control algorithm for the longitudinal model of a generic airbreathing hypersonic flight vehicle hypersonic flight vehicle. The mature LQR controller is used to stabilize the attitude of hypersonic vehicle in this paper.

In this study, on the basis of the one-dimensional engine model and the nonlinear longitudinal dynamics model of a hypersonic vehicle, an airframe-propulsion integrated model is established. Furthermore, the attitude and height controllers of the aircraft are designed. Finally, through simulation examples, the coupling characteristics of the aircraft and engine are analyzed and the conclusions are drawn.

2. Airframe-propulsion integrated model

Fig. 1 shows the geometry of the airbreathing hypersonic vehicle adopted in this work. The scramjet is placed in the underbelly of the aircraft. The lower wall of the aircraft front serves as the compression surface of the engine inlet. The rear lower wall surface serves as the free expansion surface to obtain greater thrust. Such a geometric configuration is typical for airbreathing hypersonic vehicles.

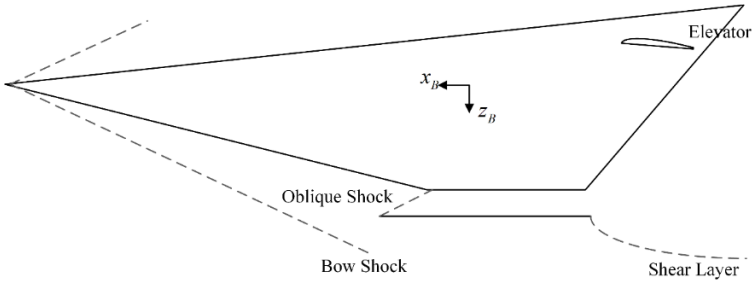

Fig. 1 Geometric configuration of airbreathing hypersonic vehicles

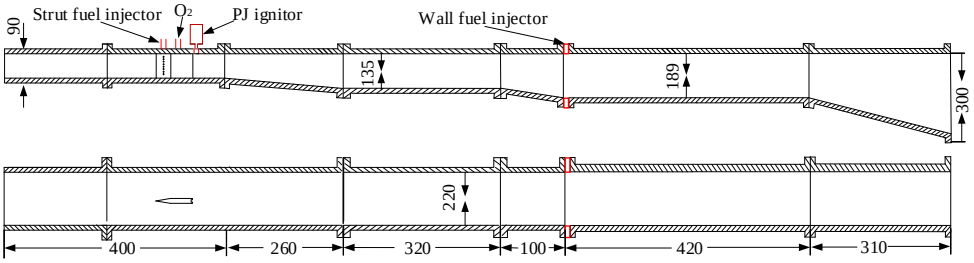

Fig. 2 Schematic diagram of engine configuration

2.1 Nonlinear longitudinal dynamical model of an airbreathing hypersonic vehicle

Mirmirani and Bolender (2007) of the U.S. Air Force laboratory proposed an analytical model of a hypersonic vehicle based on the oblique shock theory, Prandtl-Meyer expansion wave theory, and computational fluid dynamics. Furthermore, Parker fitted the expressions of forces and moments in the analytical model with polynomials, thereby obtaining a control-oriented model that can be expressed as follows

$$\begin{gathered}\dot{V} = \frac{Th\cos\alpha - D}{m} - g\sin(\theta-\alpha) \quad \dot{\alpha} = -\frac{1}{mV}(L + Th\sin\alpha) + q + \frac{g}{V}\cos(\theta-\alpha) \\ \dot{h} = V\sin(\theta-\alpha) \quad \dot{\theta} = q \quad \dot{q} = \frac{M}{I_{yy}}\end{gathered} \tag{1}$$

The longitudinal dynamics model of the aircraft has five system state variables $x = [V \quad \alpha \quad h \quad \theta \quad q]^T$. The control input δ_e does not appear explicitly in the equations of motion. Instead, it enters through the forces and moments Th, D, L, M. The thrust is provided by the engine model. The longitudinal aerodynamic forces and moments are described by

$$L = \bar{q}SC_L(\alpha,\delta_e) \quad D = \bar{q}SC_D(\alpha,\delta_e) \quad M = z_T Th + \bar{q}S\bar{c}C_M(\alpha,\delta_e) \tag{2}$$

2.2 Dual-mode scramjet model

A one-dimensional model of a scramjet engine for control and real-time simulation was established by Ma (2019) from the Harbin Institute of Technology. By calculating the internal flow field structure of the engine, the engine thrust and steady margin are obtained. The model can reflect the unsteady characteristics of the flow field and the characteristics of the parameter distributions. The engine geometry is shown in Fig. 2.

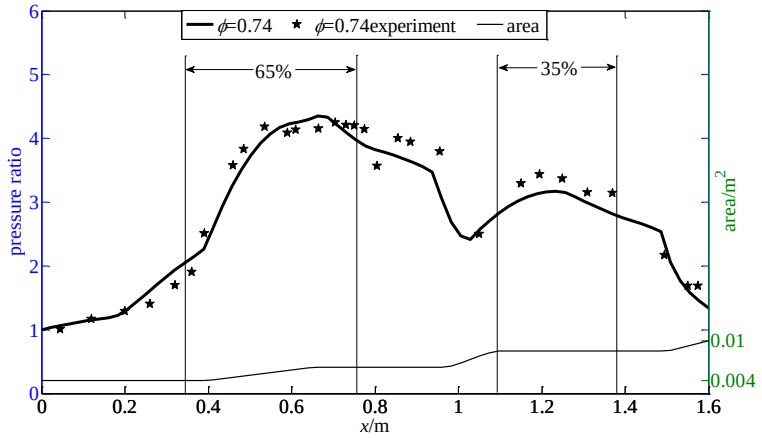

Fig. 3 Fuel equivalence ratio ϕ = 0.74; comparison of experimental and calculated stress distribution

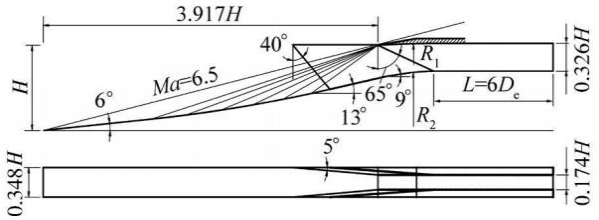

Fig. 4 Aerodynamic layout of inlet

Table 1 Total pressure recovery coefficient and Mach at the inlet of the isolator vary with the angle of attack

Mach	Mach at different angles of attack						Total pressure recovery coefficient at different angles of attack					
	-2°	0°	2°	4°	6°	8°	-2°	0°	2°	4°	6°	8°
4	1.85	1.76	1.66	1.56	1.45	—	0.693	0.692	0.691	0.683	0.664	—
5	2.35	2.25	2.15	2.05	1.92	1.79	0.594	0.59	0.579	0.561	0.532	0.493
6	2.71	2.61	2.51	2.41	2.26	2.11	0.519	0.504	0.478	0.439	0.401	0.358
7	2.88	2.78	2.66	2.54	2.39	2.24	0.442	0.388	0.337	0.291	0.254	0.228

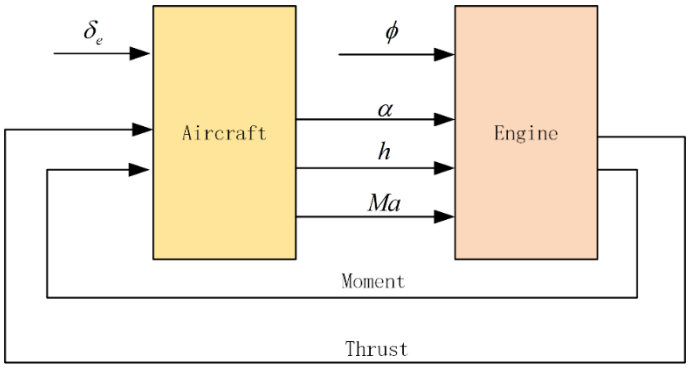

Fig. 5 Aircraft/engine integration model

The engine simulation results are presented in the Fig. 3, which shows the pressure distribution along the path. The inlet condition of isolation is Mach 2, the total temperature is 1480 K, and the static pressure is 0.059 MPa. The proportion of the first stage fuel is 0.65, and that of the second stage fuel is 0.35.

In this study, an inlet module is added to the engine model to ensure the integrity of the engine model. The inlet geometry is shown in Fig. 4. Through computational fluid dynamics (CFD) calculations, we obtained the total pressure recovery coefficient and Ma at the inlet of the isolator under different Mach numbers and angles of attack, as is shown in Table 1. The total pressure recovery coefficient of the inlet represents the ratio of the total air pressure at the outlet of the inlet to the total air pressure at the undisturbed section. Finally, the input and output of the engine model are shown in Fig. 5.

2.3 Integrated model of aircraft and engine

The integrated model of the aircraft and engine is shown in Fig. 5. The key aspects of the integrated model are the transfer variables between the aircraft and the engine. The engine provides thrust and moment for the aircraft, and the aircraft provides intake conditions for the engine. Therefore, the transfer variables between the aircraft and the engine are thrust, moment, angle of attack, altitude, and Ma.

3. Analysis of airframe-propulsion coupling characteristics

Time domain simulations are required to analyze the coupling characteristics of the aircraft/engine integrated model, and the hypersonic aircraft itself is a statically unstable system, such that the controller of the aircraft must be introduced in the coupling characteristic analysis to ensure the stable flight of the aircraft. Therefore, this chapter first presents the design of the aircraft controller, followed by an analysis of the integrated coupling characteristics.

3.1 Aircraft controller design

The nonlinear state equation of a hypersonic vehicle is denoted as follows:

$$\dot{X}_v = [f_V(X_v, U_v), \quad f_\alpha(X_v, U_v), \quad f_h(X_v, U_v), \quad f_\theta(X_v, U_v), \quad f_q(X_v, U_v)]^T \tag{3}$$

In a general integrated model, the engine thrust is further expressed as a function of the fuel equivalent ratio in an analytical form. This modeling method is suitable for aircraft control under normal engine operation. Considering that the integrated coupling characteristic analysis should be carried out and the characteristics of the engine should be fully considered, the engine characteristics were not included in the aircraft controller design process, and the thrust was taken as the transfer variable between the aircraft and the engine. The control variable of the aircraft model is set as $u_{v1} = \delta_e$.

The model trim point is shown in Table 2. Near the balance point, the linearized equation is described as follows:

$$\dot{X}_v = A_v X_v + B_v u_{v1} \tag{4}$$

In order to realize the aircraft height tracking function, the integral of aircraft height tracking

Table 2 Trim point for aircraft model

State	Value	Units
Ma	4.8	—
α	0.2	deg
h	2100.	m
θ	0.2	deg
q	0	deg/s

error is selected as a new state variable, which is denoted as

$$\dot{w} = h_r - h = h_r - C_v X_v, \quad C_v = [0 \quad 0 \quad 1 \quad 0 \quad 0] \tag{5}$$

In this work, it is assumed that the rigid body dynamic system of the aircraft can be fully state feedback (Colgren *et al.*1999, Baumann *et al*. 2010).

The trim point is $X_{v,0} = [V_0 \quad \alpha_0 \quad h_0 \quad \theta_0 \quad q_0]'$, $u_{v1,0} = \delta_{e,0}$. The new state variable of the aircraft is the deviation between the aircraft state and the trim point. The new control variable of the aircraft is the deviation between the control variable of the aircraft and the trim point. The state equation of the linearized system is expressed in an incremental form as follows:

$$\begin{cases} \bar{X}_v = X_v - X_{v,0} \\ \bar{u}_{v1} = u_{v1} - u_{v1,0} \end{cases} \tag{6}$$

After variable substitution, the aircraft stability and height tracking control problem is transformed into a typical linear quadratic optimal state controller design problem. The form of the augmented system is shown as follows:

$$\begin{gathered} \dot{w} = -C_v \bar{X}_v \\ \Downarrow \\ \begin{bmatrix} \dot{\bar{X}}_v \\ \dot{w} \end{bmatrix} = \begin{bmatrix} A_v & 0_{5\times1} \\ -C_v & 0 \end{bmatrix} \begin{bmatrix} \bar{X}_v \\ w \end{bmatrix} + \begin{bmatrix} b_{v1} \\ 0 \end{bmatrix} \bar{u}_{v1} \\ \Downarrow \\ \dot{\bar{X}}_{v,aug} = A_{v,aug} \bar{X}_{v,aug} + b_{v,aug} \bar{u}_{v1} \end{gathered} \tag{7}$$

The above control objectives are expressed as quadratic performance indicators

$$J\left(\bar{X}_{v,aug}, \bar{u}_{v1}\right) = \frac{1}{2} \int_0^\infty \left[\bar{X}'_{v,aug}(t) Q \bar{X}_{v,aug}(t) + \bar{u}'_{v1}(t) R \bar{u}_{v1}(t)\right] dt \tag{8}$$

where $Q = Q^T \geq 0$, $R = R^T \geq 0$

The optimization problem expressed in formula (8) is an extremal problem with an equation-constrained functional, and the dynamic equations of the augmented system are equation-constrained, as follows:

$$f\left(\bar{X}_{v,aug}, \bar{u}_{v1}, t\right) - \dot{\bar{X}}_{v,aug} = 0 \tag{9}$$

Lagrange multipliers are introduced to construct a generalized functional:

$$\begin{aligned} J_a &= \int_0^{\infty} L\left(\bar{X}_{v,aug}, \bar{u}_{v1}, t\right) + \lambda'(t)\left[f\left(\bar{X}_{v,aug}, \bar{u}_{v1}, t\right) - \dot{\bar{X}}_{v,aug}\right] dt \\ &= \int_0^{\infty} \left[H\left(\bar{X}_{v,aug}, \bar{u}_{v1}, t\right) - \lambda(t)\dot{\bar{X}}_{v,aug}\right] dt \end{aligned} \tag{10}$$

The Hamiltonian is defined as:

$$H = L + \lambda'(t) f\left(\bar{X}_{v,aug}, \bar{u}_{v1}, t\right) = L + \lambda'(t)\left[A_{v,aug}\bar{X}_{v,aug} + b_{v,aug}\bar{u}_{v1}\right] \tag{11}$$

According to the minimum principle of a continuous system, aiming at the following problem:

$$\begin{aligned} \underset{\bar{u}_{v1}(t)}{Extremize} J &= \int_0^{\infty} L\left(\bar{X}_{v,aug}, \bar{u}_{v1}, t\right) dt \\ s.t. \quad & f\left(\bar{X}_{v,aug}, \bar{u}_{v1}, t\right) - \dot{\bar{X}}_{v,aug} = 0 \\ & \bar{X}_{v,aug}(0) = \bar{X}_{v,aug,0} \end{aligned} \tag{12}$$

The necessary conditions to realize the optimal control are as follows:
1) The optimal state and the optimal co-state satisfy the canonical equation

$$\dot{\bar{X}}_{v,aug} = \frac{\partial H}{\partial \lambda} \quad \dot{\lambda} = -\frac{\partial H}{\partial \bar{X}_{v,aug}} \tag{13}$$

2) The optimal control satisfies the governing equation

$$\frac{\partial H}{\partial \bar{u}_{v1}} = 0 \tag{14}$$

Expand the regular equation and the governing equation in turn

$$\begin{aligned} \dot{\bar{X}}_{v,aug} &= \frac{\partial H}{\partial \lambda} = A_{v,aug}\bar{X}_{v,aug} + b_{v,aug}\bar{u}_{v1} \\ \dot{\lambda} &= -\frac{\partial H}{\partial \bar{X}_{v,aug}} = -\left[Q\bar{X}_{v,aug} + A'_{v,aug}\lambda\right] \\ \frac{\partial H}{\partial \alpha^{F_2}} &= R\bar{u}_{v1} + b'_{v,aug}\lambda = 0 \end{aligned} \tag{15}$$

The optimal solution of the control quantity can be obtained as follows:

$$\bar{u}_{v1} = -R^{-1}b'_{v,aug}\lambda \tag{16}$$

Suppose $\lambda(t)$ has the following form:

$$\lambda(t) = P(t)\bar{X}_{v,aug}(t) \tag{17}$$

There exist

$$\dot{\lambda}(t) = \dot{P}(t)\bar{X}_{v,aug}(t) + P(t)\dot{\bar{X}}_{v,aug}(t) \tag{18}$$

When we substitute Eqs. (17) and (18) into formula (15), we obtain two different forms of differential equations for Lagrange multipliers $\lambda(t)$

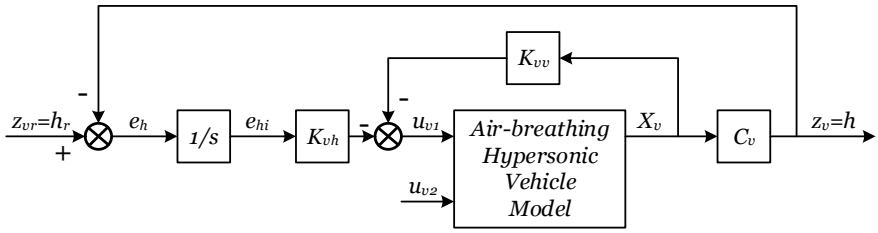

Fig. 6 Aircraft stabilization/tracking controller structure

$$\begin{aligned}\dot{\lambda} &= -\left(Q + A'_{v,aug}P\right)\bar{X}_{v,aug} \\ \dot{\lambda} &= \left(\dot{P} + PA_{v,aug} - Pb_{v,aug}R^{-1}b'_{v,aug}P\right)\bar{X}_{v,aug}\end{aligned} \tag{19}$$

The differential Riccati equation of P is reduced to the algebraic Riccati equation

$$Q + PA_{v,aug} + A'_{v,aug}P - Pb_{v,aug}R^{-1}b'_{v,aug}P = 0 \tag{20}$$

$P = P'$ is the only solution to the algebraic Riccati equation.

The complete structure of the aircraft controller can be obtained as follows:

$$\begin{aligned}u_{v1} &= u_{v1,0} - K_v\bar{X}_{v,aug} \\ &= u_{v1,0} - [K_{vv} \quad K_{vh}]\left[\left(X_v - X_{v,0}\right) \quad w\right]' \\ &= u_{v1,0} - K_{vv}\left(X_v - X_{v,0}\right) - K_{vh}\int(z_{vr} - C_vX_v)dt\end{aligned} \tag{21}$$

The controller structure is often referred to as a linear quadratic proportional integral filter structure (Huo *et al*. 2006, Kuipers *et al*. 2007, Stengel 2015). K_{vv} is used to control attitude stability, which ensures that the pitching rate of the aircraft is controlled near zero. K_{vh} is used to control altitude tracking, which realizes the flight of the aircraft along the trajectory of the specified altitude. The aircraft control loop is shown in Fig. 6.

A simulation is carried out to verify the control effect of the aircraft controller. The flight starts at Ma = 5, h = 22.03 km. The control objective is to first climb under constant pressure for 20 s, and then cruise at constant altitude for 10 s. The simulation results show the changes in altitude, velocity, and flight attitude. The altitude tracking has a delay of approximately 2 s. The angle of attack and flight path angle change only when the aircraft state changes. The attitude of the aircraft remained stable for the rest of the time, indicating that the attitude control effect of the aircraft was good.

3.2 Analysis of airframe-propulsion coupling characteristics

In this study, a case of ignoring the coupling between the aircraft and the engine was set up for a comparative analysis with the normal case. The interaction between the working condition of the engine and the attitude of the vehicle is analyzed. In the simulation ignoring the coupling, the attitude of the aircraft has no effect on the working condition of the engine; that is, the intake flow of the engine is not affected by the flight angle of attack, but only by the altitude and Mach number. Moreover, the attitude of the aircraft is not affected by the working condition of the

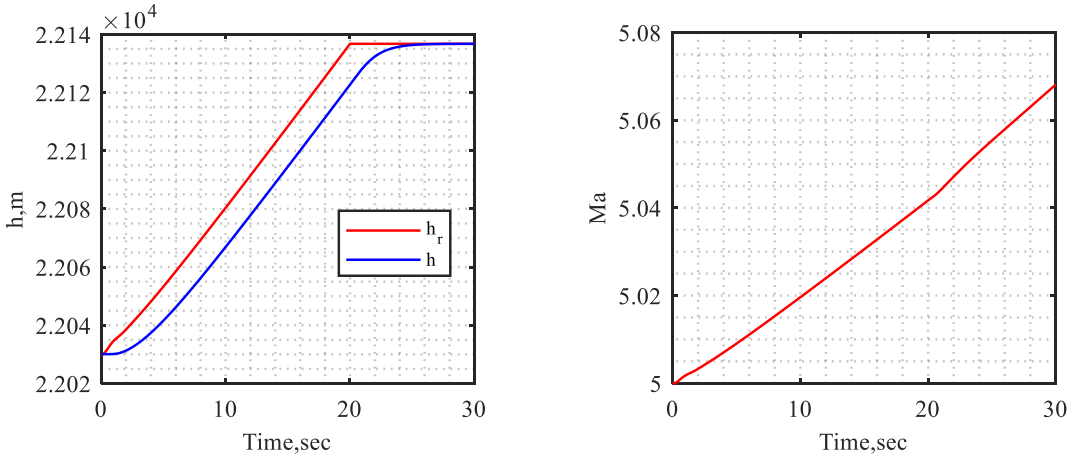

(a) Altitude (b) Ma

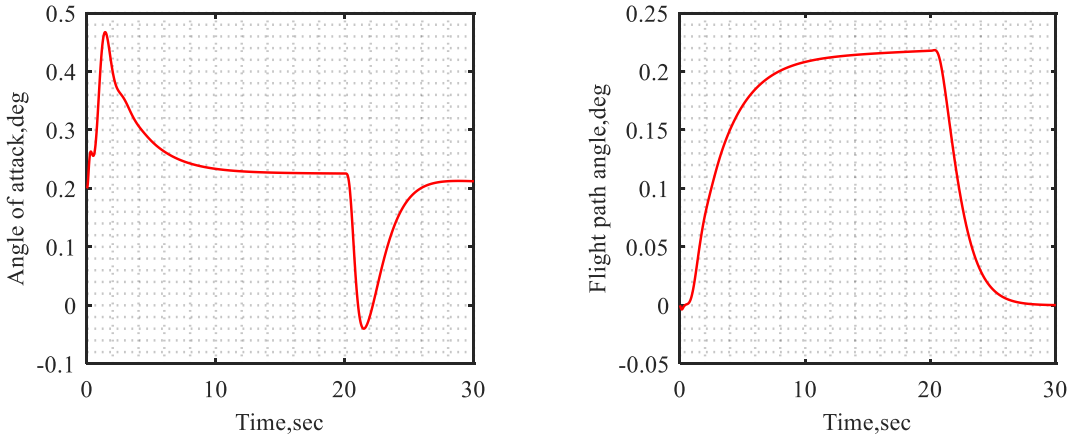

(c) Angle of attack (d) Fight path angle

Fig. 7 Simulation results of aircraft control effect

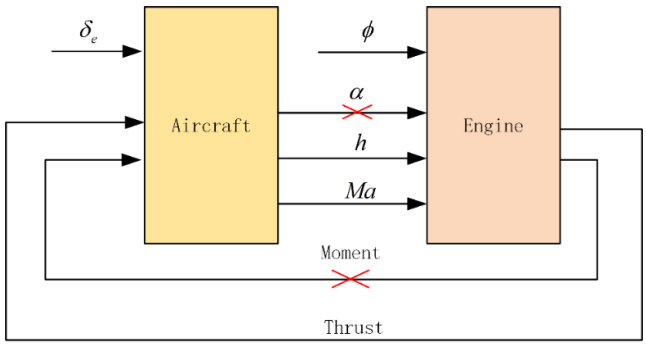

Fig. 8 Integration model that ignores coupling

engine; that is, the thrust moment of the aircraft is constant and does not change with the engine thrust. The integration model that ignores coupling is shown in Fig. 8.

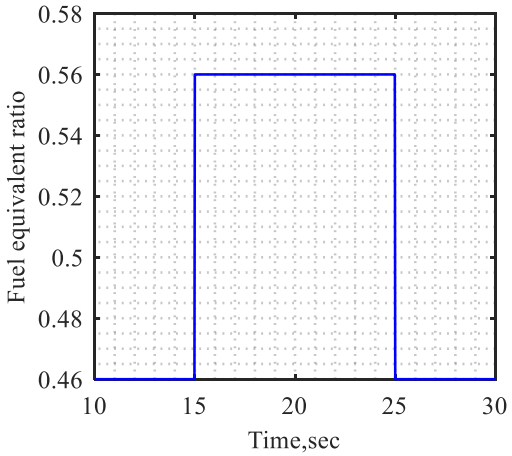

(a) Fuel equivalent ratio

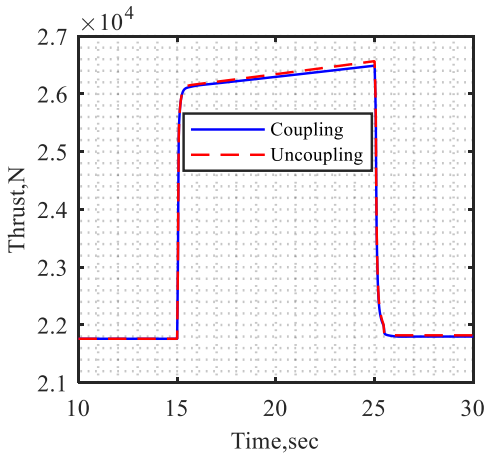

(b) Thrust

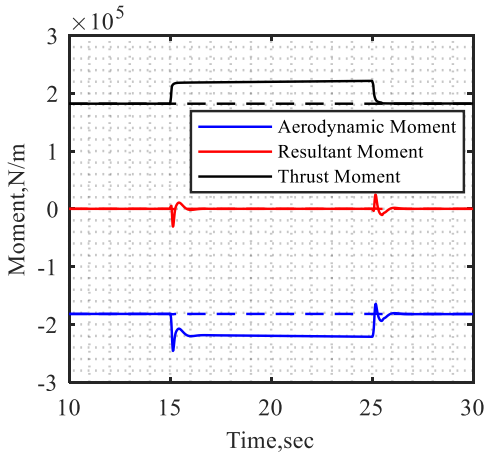

(c) Moment

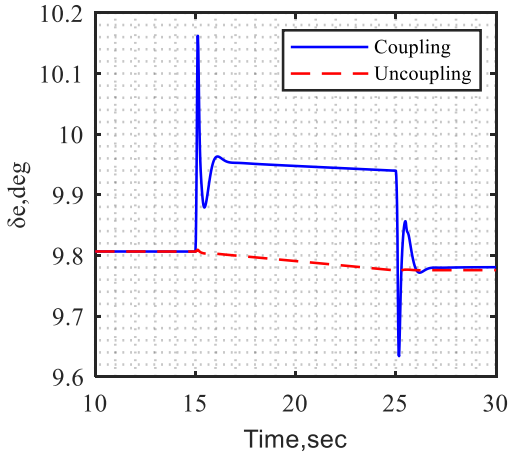

(d) δ_e

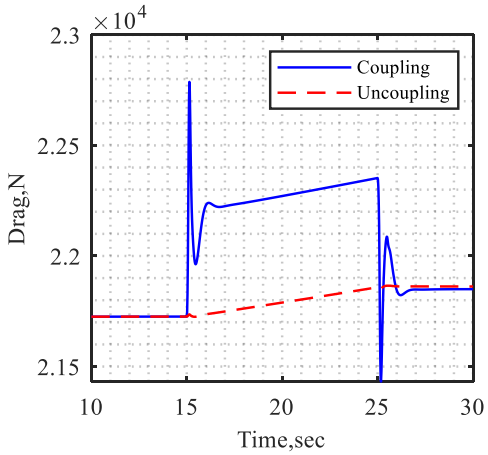

(e) Drag

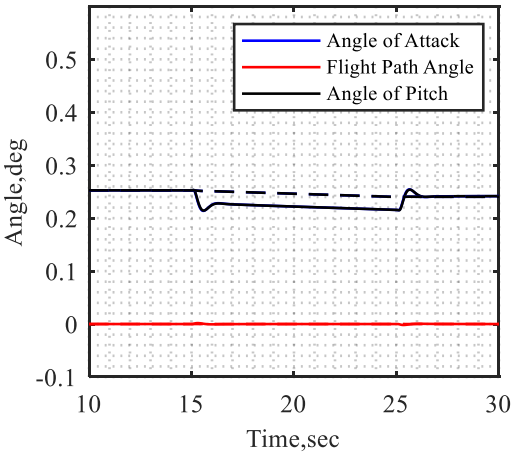

(f) Angle of attack, flight path angle, and angle of pitch

Fig. 9 Parameters of aircraft and engine under changing engine working conditions

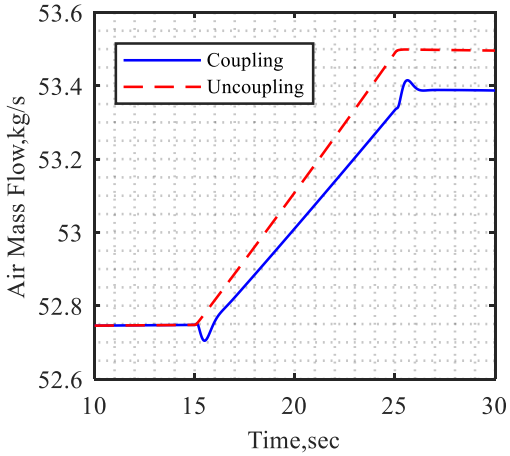

(g) Air mass flow

Fig. 9 Continued

3.2.1 Influence of engine working conditions on vehicle attitude

Our research focuses on the modeling and coupling characteristics analysis for an airframe-propulsion-integrated hypersonic vehicle in specified operating condition. The engine model adopted in coupling system is a scramjet with regenerative cooling function, which has two-stage fuel equivalent ratio adjustment to deal with inlet unstart and combustor overtemperature problem (Ma *et al.* 2019). However, the coupling characteristics discussed in this paper occur at the specified cruising condition. According to the matching of aircraft model and engine model, this condition is not close to any engine safety boundary such as inlet unstart, combustor overtemperature, etc. Thus, the second-stage fuel equivalent ratio does not need to be adjusted with a value of 0 (Ma *et al.* 2019). In further research, we will consider the acceleration of the integrated system, where the second-stage fuel equivalent ratio will play an important role in safety regulation. The first-stage fuel equivalent ratio is set according to the flight conditions and coupling system matching. Therefore, the operating point is selected as Ma = 6, h = 24 km, the fuel equivalent ratio of the first stage is 0.33, the fuel equivalent ratio of the second stage is 0, and the aircraft was cruising at the same altitude. At t = 15 s, the fuel equivalent ratio of the first stage increased by 0.25, and at t = 25 s, the fuel equivalent ratio of the first stage decreased by 0.25. The fuel equivalent ratio of the second stage remained unchanged. The simulation lasted for 30 s and the conditions of the aircraft and engine change as shown in Fig. 9.

As can be seen from Fig. 9(b), when the fuel equivalent ratio increases and decreases, the engine thrust significantly increases and decreases, respectively. The moment of the vehicle also changes markedly when coupling is considered. This is because the change in thrust leads to a change in thrust moment, and the aircraft's moment balance is broken. However, without considering the coupling, the moment remains unchanged, as shown in Fig. 9(c).

The change in moment leads to an instability of the attitude of the aircraft. The aircraft controller adjusts the aerodynamic moment by adjusting the elevator angular deflection to maintain the resultant moment near 0. As shown in Fig. 9(d), δ_e changes significantly at 15 and 25 s. The drag changes are shown in Fig. 9(e). Under the influence of coupling, the angle of attack

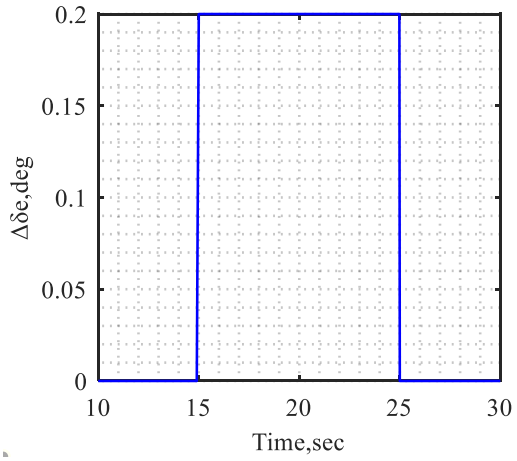

(a) $\Delta\delta_e$

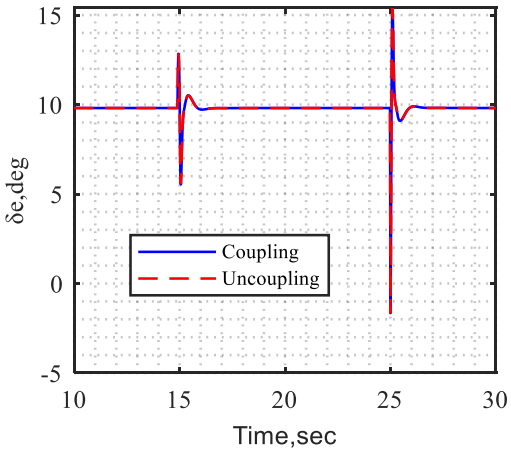

(b) δ_e

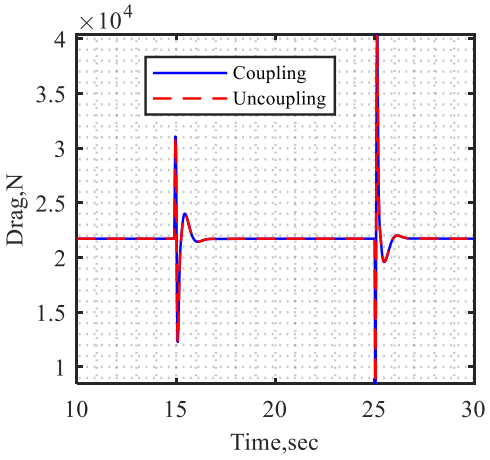

(c) Drag

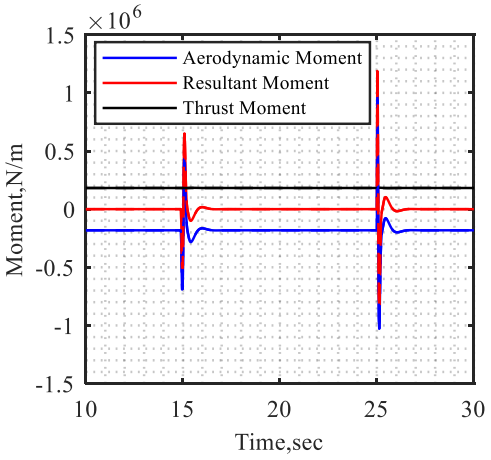

(d) Moment

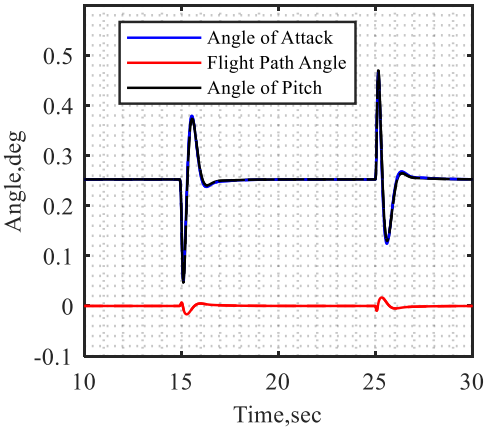

(e) Angle of attack, flight path angle, and angle of pitch

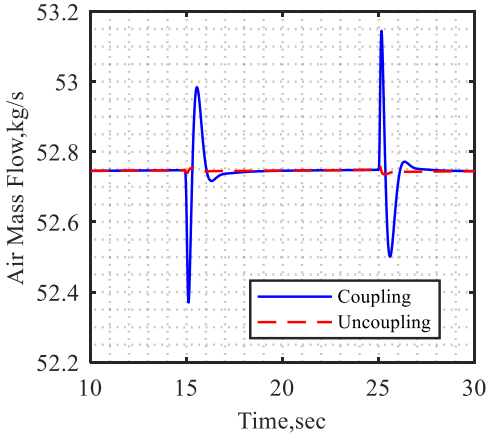

(f) Air mass flow

Fig. 10 Parameters of the aircraft and the engine under changing vehicle attitude

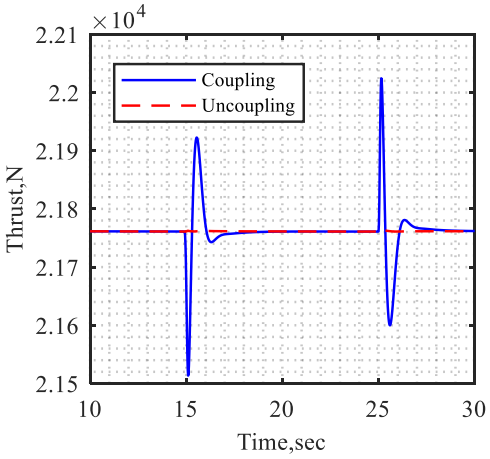

(g) Thrust

Fig. 10 Continued

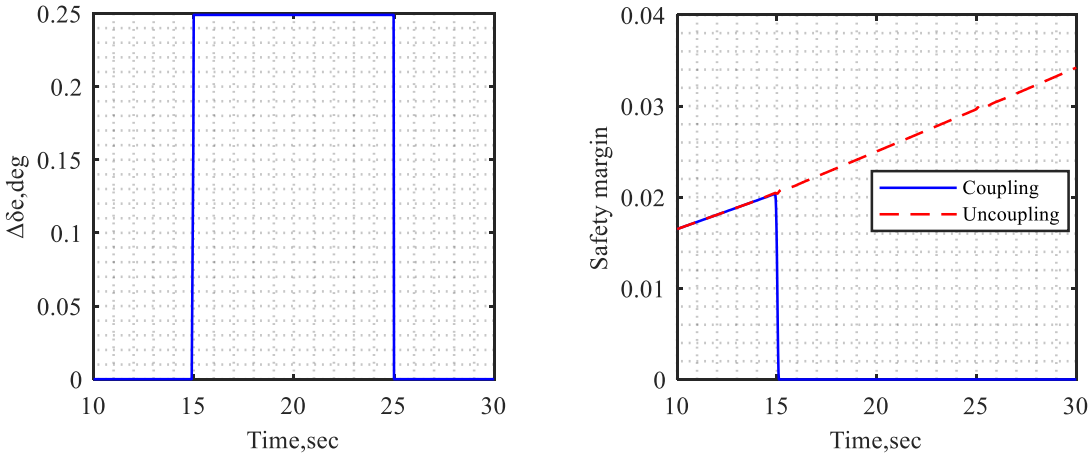

(a) $\Delta\delta_e$ (b)Safety margin

Fig. 11 Influence of vehicle attitude on engine safety

and angle of pitch change slightly, whereas without considering coupling, the angle of attack and angle of pitch do not change. This also indicates that the coupling characteristics cause the working conditions of the engine to affect the attitude of the aircraft. It can be seen from Fig. 9(g) that the air flow of the engine without coupling is greater than that with coupling, because the coupling makes the aircraft's angle of attack decrease, which leads to a decrease in air flow, as can be seen from Fig. 9(f).

In summary, when the working conditions of the engine are changed, the original moment balance of the aircraft is broken. Under the action of the aircraft controller, the aircraft works stably at the new equilibrium point.

3.2.2 Influence of vehicle attitude on engine working condition

When analyzing the coupling characteristics, the operating point is selected as Ma = 5, h = 22

km, the fuel equivalent ratio of the first stage is 0.33, and the fuel equivalent ratio of the second stage is 0. The aircraft cruises at the same altitude. From t = 15 s to t = 25 s, δ_e is disturbed and rises 0.2°. The simulation lasted for 30 s, and the conditions of the aircraft and engine change as shown in Fig. 10.

It can be seen from Fig. 10(b) that δ_e quickly returns to the normal state after being disturbed. Fig. 10(d) shows that the moment balance of the aircraft is broken in a short time when δ_e changes. The resultant moment is then stabilized near 0 by adjusting δ_e. It can be seen from Fig. 10(e) that the angles of attack and pitch also fluctuate during attitude adjustment. Under the coupling effect, the attitude of the aircraft changes, resulting in a change in the engine inlet flow, and in turn causing a fluctuation in the engine thrust. However, as the attitude of the aircraft stabilizes, the thrust fluctuation gradually decreases and finally stabilizes. Changes in the air flow and thrust can be seen in Fig. 10(f) and 10(g).

To summarize, when the attitude of the aircraft changes, the inlet flow of the engine will change, which will lead to a change in the thrust. As the attitude of the aircraft is stabilizes, the engine will gradually restore stability.

3.2.3 Effects of coupling characteristics on engine safety

The previous simulations were performed at lower fuel equivalent ratios. The engine has a higher safety margin when the fuel equivalent ratio is low. The coupling characteristics have no significant impact on engine safety. Now, consider the engine operating in a lower-margin state; that is, the engine has a higher fuel equivalent. The operating point is selected as Ma = 5, h = 22km, the fuel equivalent ratio of the first stage is 0.56, and the fuel equivalent ratio of the second stage is 0. The aircraft cruises at the same altitude. From t = 15 s to t = 25 s, δ_e is disturbed and rises 0.25°. The simulation lasted for 30 s, and the conditions of the aircraft and engine change as shown in Fig. 11.

As shown in Fig. 11, the engine safety margin continues to increase when coupling is taken into account. This is because the aircraft is accelerating at a high fuel equivalent ratio. The higher the incoming flow velocity, the greater the combustor backpressure that the isolation section can withstand, the less easily the shock wave string can be pushed out, and the greater the engine margin, such that the engine margin continues to rise. However, in the case of coupling, engine unstart already occurs at t = 15 s. As can be seen from Fig. 11(b), the engine safety margin is 0. Therefore, in the design of an airbreathing hypersonic vehicle, the influence of coupling should be fully considered.

4. Conclusions

It is a very complicated task to build an integrated model of a hypersonic aircraft/scramjet. On the basis of the traditional flight mechanics modeling theory, we must establish a scramjet model that can accurately reflect the engine characteristics and the strong coupling model oriented to the airframe-propulsion integration. The conclusions are summarized as follows:

• In this paper, an airframe-propulsion integration model is established based on the one-dimensional engine model. The integration model fully embodies the coupling relationship between the aircraft and the engine. Through a simulation example, the validity of the modeling is verified. The integrated model exhibits both accuracy and rapidity, and is suitable for the research of hypersonic aircraft integration. Its rationality and feasibility render it of great value for

engineering applications.

• The coupling relationship between the engine working conditions and the aircraft attitude is revealed. When the working conditions of the engine change, the moment balance of the aircraft is broken. The aircraft controller adjusts the aerodynamic moment by adjusting the elevator angular deflection to maintain the resultant moment near 0. When the vehicle attitude changes, it leads to a change in the engine intake flow, which in turn causes a change in thrust. However, owing to the existence of the aircraft controller, with the stability of the aircraft attitude, the working thrust of the engine gradually returns to stability.

• When the engine is working in the critical state, if the coupling characteristics are not considered, the engine's working state may be misjudged. The engine unstarting condition is disastrous, and should be avoided as much as possible. In the design of an airbreathing hypersonic vehicle, the influence of coupling should be fully considered.

Acknowledgments

This research work is supported by the National Science and Technology Major Project (2017-V-0004-0054).

References

Andrew, C., Chivey, W. and Maj, M. (2006), "Development of an airframe-propulsion integrated generic hypersonic vehicle model", *Proceedings of the 44th AIAA Aerospace Sciences Meeting and Exhibit*, Reno, Nevada, U.S.A., January.

Baumann, E., Pahle, J.W., Davis, M.C. and White, J.T. (2010), "X-43A flush airdata sensing system flight-test results", *J. Spacecraft Rockets*, **47**(1), 48-61. https://doi.org/10.2514/1.41163.

Bharani Chandra, K.P., Gupta, N.K., Ananthkrishnan, N., Park, I.S. and Yoon, H.G. (2010), "Modeling, simulation, and controller design for an air-breathing combustion system", *J. Propul. Power*, **26**(3), 562-574. https://doi.org/10.2514/1.42368.

Bilimoria, K.D. and Schmidt, D.K. (1995), "Integrated development of the equations of motion for elastic hypersonic flight vehicles", *J. Guid. Control Dynam.*, **18**(1), 73-81. https://doi.org/10.2514/3.56659.

Bolender, M. and Doman, D. (2005), "A non-linear model for the longitudinal dynamics of a hypersonic air-breathing vehicle", *Proceedings of the AIAA Guidance, Navigation, and Control Conference and Exhibit*, San Francisco, California, U.S.A., August.

Bolender, M.A. and Doman, D.B. (2007), "Nonlinear longitudinal dynamical model of an air-breathing hypersonic vehicle", *J. Spacecraft Rockets*, **44**(2), 374-387. https://doi.org/10.2514/1.23370.

Burcham, Jr, F., Ray, R., Conners, T. and Walsh, K. (1998), "Propulsion flight research at NASA Dryden from 1967 to 1997", *Proceedings of the 34th AIAA/ASME/SAE/ASEE Joint Propulsion Conference and Exhibit*, Cleveland, U.S.A., July.

Chavez, F.R. and Schmidt, D.K. (1994), "Analytical aeropropulsive-aeroelastic hypersonic-vehicle model with dynamic analysis", *J. Guid. Control Dynam.*, **17**(6), 1308-1319. https://doi.org/10.2514/3.21349.

Colgren, R., Frye, M. and Olson, W. (1999), "A proposed system architecture for estimation of angle-of-attack and sideslip angle", *Proceedings of the AIAA Guidance, Navigation, and Control Conference and Exhibit*, Portland, Oregon, U.S.A., August.

Cui, T. (2014), "Simplified procedure for controlling pressure distribution of a scramjet combustor", *Chin. J. Aeronaut.*, **27**(5), 1137-1141. https://doi.org/10.1016/j.cja.2014.08.015.

Cui, T., Yu, D.R. and Bao, W. (2008), "Distributed parameter control arithmetic for an axisymmetrical dual-mode scramjet", *Aeronaut. J.*, **112**(1135), 557-565. https://doi.org/10.1017/S0001924000002517.

Groves, K.P., Sigthorsson, D.O., Yurkovich, S., Bolender, M.A. and Doman. D.B. (2005), "Reference command tracking for a linearied model of an air-breathing hypersonic vehicle", *Proceedings of the AIAA Guidance, Navigation and Control Conference and Exhibit*, San Francisco, California, U.S.A., August.

Groves, K.P., Serrani, A., Yurkovich, S., Bolender, M.A. and Doman. D.B. (2006), "Anti-windup control for an air-breathing hypersonic vehicle model", *Proceedings of the AIAA Guidance, Navigation and Control Conference and Exhibit*, Keystone, Colorado, U.S.A., August.

Hank, J., Murphy, J. and Mutzman, R. (2007), "The X-51A scramjet engine flight demonstration program", *Proceedings of the 15th AIAA International Space Planes and Hypersonic Systems and Technologies Conference*, Dayton, Ohio, U.S.A., April.

Huo, Y., Mirmirani, M., Ioannou, P. and Kuipers, M. (2006), "Altitude and velocity tracking control for an airbreathing hypersonic cruise vehicle", *Proceedings of the AIAA Guidance, Navigation and Control Conference and Exhibit*, Colorado, U.S.A., August.

Kuipers, M., Mirmirani, M., Ioannou, P. and Huo, Y. (2007), "Adaptive control of an aeroelastic airbreathing hypersonic cruise vehicle", *Proceedings of the AIAA Guidance, Navigation and Control Conference and Exhibit*, Hilton Head, South Carolina, U.S.A., August.

Lee, Y.J., Kang, S.H. and Yang, S.S. (2015), "A study on the hypersonic air-breathing engine ground test facility composition and characteristics", *J. Kor. Soc. Propul. Eng.*, **19**(6), 81-90. https://doi.org/10.6108/KSPE.2015.19.6.081.

Liu, Y. and Hua, B. (2015), "Compromise optimal design using control-based analysis of hypersonic vehicles", *Int. J. Aeronaut. Space Sci.*, **16**(2), 137-147. https://doi.org/10.5139/IJASS.2015.16.2.137.

Ma, J.C., Chang, J.T., Zhang, J.L, Bao, W. and Yu, D.R. (2018), "Control-oriented modeling and real-time simulation method for a dual-mode scramjet combustor", *Acta Astronautica*, **153**, 82-94. https://doi.org/10.1016/j.actaastro.2018.10.002.

Ma, J.C., Chang, J.T., Zhang, J.L, Bao, W. and Yu, D.R. (2019), "Control-oriented unsteady one-dimensional model for a hydrocarbon regeneratively-cooled scramjet engine", *Aerosp. Sci. Technol.*, **85**, 158-170. https://doi.org/10.1016/j.ast.2018.12.012.

Ma, J.C., Chang, J.T., Huang, Q.P., Bao, W. and Yu, D.R. (2019), "Multi-objective coordinated control of regeneratively-cooled scramjet engine with two-stage kerosene injection", *Aerosp. Sci. Technol.*, **90**, 59-69. https://doi.org/10.1016/j.ast.2019.04.027.

McClinton, C. (2006), "X-43-scramjet power breaks the hypersonic barrier: Dryden lectureship in research for 2006", *Proceedings of the 44th AIAA Aerospace Sciences Meeting and Exhibit*, Reno, Nevada, U.S.A., January.

Mitani, T., Hiraiwa, T., Sato, S., Tomioka, S., Kanda, T. and Tani, K. (1997), "Comparison of scramjet engine performance in Mach 6 vitiated and storage-heated air", *J. Propul. Power*, **13**(5), 635-642. https://doi.org/10.2514/2.5228.

Parker, J.T., Serrani, A., Yurkovich, S., Bolender, M.A. and Doman, D.B. (2007), "Control-oriented modeling of an air-breathing hypersonic vehicle", *J. Guid. Control Dynam.*, **30**(3), 856-869. https://doi.org/10.2514/1.27830.

Roux, J.A. and Tiruveedula, L.S. (2016), "Constant velocity combustion parametric ideal scramjet cycle analysis", *J. Thermophys. Heat Tr.*, **30**(3), 698-704. https://doi.org/10.2514/1.T4792.

Shen, H.D., Liu, Y.B., Chen, B.Y. and Lu, Y.P. (2018), "Control-relevant modeling and performance limitation analysis for flexible air-breathing hypersonic vehicles", *Aerosp. Sci. Technol.*, **76**, 340-349. https://doi.org/10.1016/j.ast.2018.02.016.

Smith, R.H., Chisholm, J.D. and Stewart, J.F. (1990), "Optimizing aircraft performance with adaptive, integrated flight/propulsion control", *Proceedings of the ASME 1990 International Gas Turbine and Aeroengine Congress and Exposition*, Brussels, Belgium, June.

Stengel, R. F. (2015), *Flight Dynamics*, Princeton University Press, U.S.A.

Wang, F., Guo, Y., Wang, K., Zhang, Z., Hua, C.C. and Zong, Q. (2019), "Disturbance observer based robust backstepping control design of flexible air-breathing hypersonic vehicle", *IET Control Theor. Appl.*, **13**(4), 572-583. http://doi.org/10.1049/iet-cta.2018.5482.

Wang, Y.X., Chao, T., Wang, S.Y. and Yang, M. (2019), "Trajectory tracking control of hypersonic vehicle

considering modeling uncertainty", *Proc. Inst. Mech. Eng. Part G J. Aerosp. Eng.*, **233**(13), 4779-4787. https://doi.org/10.1177/0954410019830811.
Xu, B. (2015), "Robust adaptive neural control of flexible hypersonic flight vehicle with dead-zone input nonlinearity", *Nonlinear Dynam.*, **80**(3), 1509-1520. https://doi.org/10.1007/s11071-015-1958-8.
Yao, Z.H., Bao, W., Chang, J.T., Yu, D.R. and Tang, J.F. (2010), "Modelling for couplings of an airframe—propulsion integrated hypersonic vehicle with engine safety boundaries", *Proc. Inst. Mech. Eng. Part G J. Aerosp. Eng.*, **224**(1), 43-55. https://doi.org/10.1243/09544100JAERO618.
Zhou, H.Y., Wang, X.G. and Cui, N.G. (2019), "Glide trajectory optimization for hypersonic vehicles via dynamic pressure control", *Acta Astronautica*, **164**, 376-386. https://doi.org/10.1016/j.actaastro.2019.08.012.
Zuppardi, G. (2015), "Aerodynamic control capability of a wing-flap in hypersonic, rarefied regime", *Adv. Aircraft Spacecraft Sci.*, **2**(1), 45-56. https://doi.org/10.12989/aas.2014.2.1.045.

CC

Nomenclature

A_v	System matrix
$A_{v,avg}$	Augmented system matrix
$B_{v,avg}$	Augmented input matrix
$C_{D(\alpha,\ \delta e)}$	Drag coefficient
$C_{L(\alpha,\ \delta e)}$	Lift coefficient
$C_{M(\alpha,\ \delta e)}$	Moment coefficient
$\bar{c}$	Mean aerodynamic
D	Drag
g	Acceleration due to gravity
H	Hamilton function
H	Altitude
h_r	Altitude reference trajectory
I_{yy}	Moment of inertia
q	Pitch rate
$\bar{q}$	Dynaic presssure

S	Reference area
Th	Tripm poitn
$\bar{u}_{v,1}$	İncremental control input
V	velocity
W	Altitude tracking error
X_v	State of aircraft model
$X_{v,0}$	Trim condition
$X_{v,aug}$	İncremental state of aircraft model
x_B	Body axis corrdinate frame x direction
Z_T	Body axis coordinate frame z direction
Z_T	Thrust to moment coupling coefficient